Electronic Supplementary Material (ESI) for Materials Chemistry Frontiers.

Electronic Supplementary Information

Sandwich-type Sulfur Cathode Based on Multifunctional Ceria Hollow Spheres for High-Performance Lithium-Sulfur Battery

Jianwei Wang,[a,b] Bo Zhou,[c] Hongyang Zhao,[b] Miaomiao Wu,[b] Yaodong Yang,[b] Xiaolei Sun,[a] Donghai Wang,[d] and Yaping Du*[a,b]

[a] School of Materials Science and Engineering & National Institute for Advanced Materials, Tianjin Key Lab for Rare Earth Materials and Applications, Centre for Rare Earth and Inorganic Functional Materials, Nankai University, Tianjin 300350, China.

[b] Frontier Institute of Science and Technology, Xi'an Jiaotong University, Xi'an 710054, China.

[c] Institute of Modern Physics, Shaanxi Key Laboratory for Theoretical Physics Frontiers, Northwest University, Xi'an 710069, China.

[d] Department of Mechanical and Nuclear Engineering, Pennsylvania State University, University Park, PA 16802, USA.

* E-mail: ypdu@nankai.edu.cn

Table of Contents

S1. Preparation of Hollow CeO_2

CeO_2 hollow spheres were prepared using previously reported methods. Briefly, tetraethylorthosilcate (8 mL) was dispersed in ethanol (280 mL). A mixture of ammonium hydroxide (8.4 mL, 25%, *w*/%) and deionized water (56 mL) was added under vigorous stirring, and the mixture was stirred at room temperature for 24 h. The mixture was centrifuged (8500 rpm), and then followed by drying at 60 °C for 6 h. Typically, 100 mg of dried SiO_2 templates were dispersed in 13 mL of ethylene glycol with ultrasonication in a beaker. Cerium nitrate hexahydrate (0.5 g) and deionized water (0.75 mL) were added and stirred for 30 min, and then sealed in a 25 mL Teflon-lined stainless steel autoclave at 130 °C for 24 h. After the reaction, the autoclave was cooled down to room temperature, and then the SiO_2@CeO_2 spheres were centrifuged (10000 rpm) and washed several times with ethanol. The resulting composite was dispersed in 5 mol/L NaOH solution to obtain CeO_2 hollow spheres, hereafter referred to as "Hollow CeO_2".

S2. Preparation of *h*-CeO_2

In a typical synthesis, 365 mg of CeO_2 hollow spheres was dispersed in 65 mL Tris-buffer (pH: 8.5) under ultrasonication for 30 min to form a uniform suspension. Subsequently, 65 mg of dopamine was added under vigorous stirring, and the mixture was stirred at 30 °C for 72 h. Afterwards, the resulting composite was collected by

centrifugation (8500 rpm), then washed several times with deionized water, and then dried at 50 °C for 12 h. The resulting sample was heated to 150 °C for 1 h in a tubular furnace under Ar atmosphere at a rate of 3 °C/min, and then further heated to 600 °C for 4 h with a heating rate of 5 °C/min. The obtained composite (Hollow CeO_2@Carbon) was referred to as "*h*-CeO_2".

S3. Preparation of *h*-CeO_2/Sulfur-x

h-CeO_2 spheres were soaked into a different volume of sulfur/CS_2 solution (20 mg/mL) for 48 h, then residual solvent (CS_2) was removed under reduced pressure. The obtained sulfur-containing hybrids were dried at 50 °C under vacuum. They were further heated in a sealed autoclave to 155 °C in Ar atmosphere for 12 h, then further heated to 180 °C and kept at this temperature for 1 h to remove the sulfur particles on the outer surface of *h*-CeO_2 spheres. The obtained composites were referred to as *h*-CeO_2/Sulfur-x (x =0.7, 0.8, or 0.9, where x is the initial weight ratio of sulfur).

S4. Preparation of CNT/*h*-CeO_2 interlayer and CNT interlayer

MWCNTs (14 mg) and *h*-CeO_2 (6 mg) were mixed and dispersed in 150 mL of absolute ethanol. After high-power ultrasonication for 30 min, the mixture was poured into a 40 mm diameter vacuum filtration pan. As the filtration proceeded, a thin cross-stacked CNT film that contained *h*-CeO_2 spheres was formed, and then dried at 60 °C for 24 h. The obtained composite interlayer is referred to as CNT/*h*-CeO_2 interlayer. The

CNT interlayer was also obtained by loading 20 mg of MWCNTs following the same procedure. Finally, CNT/*h*-CeO_2 interlayer as well as CNT interlayer was punched into round disks with diameter of 12 mm. The average weight of round disks was 1.6 mg/cm^2.

S5. Preparation of *h*-CeO_2/Sulfur-x cathodes

The *h*-CeO_2/Sulfur cathodes were prepared by thoroughly mixing *h*-CeO_2/Sulfur-x, Super P and binder (PVDF) at a weight ratio of 7:2:1 in N-methy-pyrrolidinone (NMP) solution. The mixture was ground in a mortar and uniformly spread on an aluminum foil. Then, they were dried at 60 °C for 24 h in a vacuum oven to completely remove the solvent. The electrode sheets were punched into round disks with diameter of 12 mm. The average loading weight of sulfur was ~1.0 mg/cm^2.

S6. Electrochemical characterization

The lithium-sulfur batteries were assembled in CR2032 coin cell in an argon-filled glovebox with oxygen and water content below 0.1 ppm, respectively. The coin-type cells were constructed with the as-prepared *h*-CeO_2/Sulfur cathodes, microporous polypropylene film membrane (Celgard 2400) and lithium metal foil anodes. The CNT/ *h*-CeO_2 interlayer or CNT interlayer was inserted between the *h*-CeO_2/Sulfur cathode and the Celgard separator. 1.0 M lithium bis(trifluoromethanesulfonyl)imide (LiTFSI) in 1,2-dimethoxyethane (DME) and 1,3-dioxolane (DOL) (1:1 volume ratio) with the addition of $LiNO_3$ (1 wt%) was used as the electrolyte. The ratio of electrolyte and sulfur was 30

μL/mg in the coin cells. The specific capacities were calculated based on the mass of sulfur in the samples, which was determined using TGA measurements. The C-rate values were based on the theoretical capacity of sulfur (1672 mAh g^{-1}). The cycling and rate performances of lithium sulfur batteries were measured on the LAND battery testing systems at 40 °C at different current densities within the voltage window of 1.7-2.6 V *vs* Li/Li^+. The other electrochemical measures were conducted at room temperature. Cyclic voltammograms (CVs) and Electrochemical impedance spectroscopy (EIS) were performed on Autolab PGSTAT302N electrochemical workstation. The CV curves were collected at a scan rate of 0.2 mV s^{-1} between 1.7 and 2.6 V, and EIS analysis was carried out at open-circuit voltage in the range from 100 KHz to 0.01 Hz with 5.0 mV amplitude. The soft-packaged Li-S batteries were also assembled in an argon-filled glovebox, similar to the case of as-prepared coin cells. The galvanostatic experiments were tested on CHI 600E electrochemical workstation in the potential range of 1.7-2.6 V. Sulfur loading was 0.84 mg cm^{-2} (~20 cm^2 in area) and Al-plastic films were used to seal soft-packaged batteries.

S7. Structure characterization

TGA measurements were conducted on a Mettler-Toledo TGA1 thermal analyzer under air at a heating rate of 10 K min^{-1} from 30 °C to 400 °C. X-ray photoelectron spectrometry (XPS, Shimadzu, AXIS Supra) was performed to identify the surface

chemical composition and the elemental information of the *h*-CeO_2/Sulfur. BET surface area was collected on a Micromeritics sorptometer (ASAP 2020 Plus HD88) using nitrogen adsorption at 77 K. The powder X-ray diffraction (XRD, Rigaku, Smartlab3) patterns were characterized in the range of 10-60° with Cu Kα radiation (λ = 1.5406 Å) at room temperature. The microstructure and morphology of the samples were examined using transmission electron microscope (TEM, Japan, HT7700), high-resolution transmission electron microscope (HRTEM, JEOL JEM-2100Plus), scanning electron microscopy (SEM, FEI 250) and field-emission scanning electron microscopy (FESEM, SU-8010). Raman spectra were collected on a laser raman spectrometer with an excitation laser of 473 nm. UV-vis measurements were carried out using DH-2000-BAL Scan spectrophotometer.

S8. Computational method

Density functional theory (DFT) implemented in the Vienna ab initio simulation package (VASP)[1] was employed to calculate the adsorption energy between the substrate and the polysulfides, which is defined by

$$E_{ads} = E_{s+sub} - E_s - E_{sub}$$

where E_{s+sub}, E_s, and E_{sub} are the energy of the polysulfides-substrate, polysulfides, and substrate, respectively. Projector-augmented-wave (PAW) potentials are used to deal with the electron-ion interactions, and the electron exchange-correlation interactions are

carried out with generalized gradient approximation (GGA) in the scheme of Perdew-Burke-Ernzerhof.[2,3] Spin-polarized calculations are also carried out. A plane wave cutoff of 500 eV is consistently used. The optimization of the whole structures is performed using a conjugate gradient algorithm, and the atomic relaxation is terminated until the energy converges within 10^{-5} eV. Accurate exchange functionals for the vdW correlation has been used in reported articles.[4]

S9. Visualized adsorption of polysulfides

1,2-dimethoxyethane (DME) was refluxed over Na and distilled under nitrogen. Li_2S_4 was prepared by reacting commercial Li_2S and sulfur at the molar ratio of 1:3 in freshly distilled DME. The mixture was vigorously stirred for 24 h and the Li_2S_4 solutions (5.0 mmol L^{-1}) were prepared by dilution. *h*-CeO_2 (4.0 mg) and *h*-CeO_2-CNT/*h*-CeO_2 (4.0 mg) were added to 2.0 mL of Li_2S_4/DME solutions, respectively. The different adsorbents in sealed vials were kept for 12 h after vigorously shaking, and then the supernatants were used for UV-vis test.

S10. N_2 adsorption-desorption isotherms

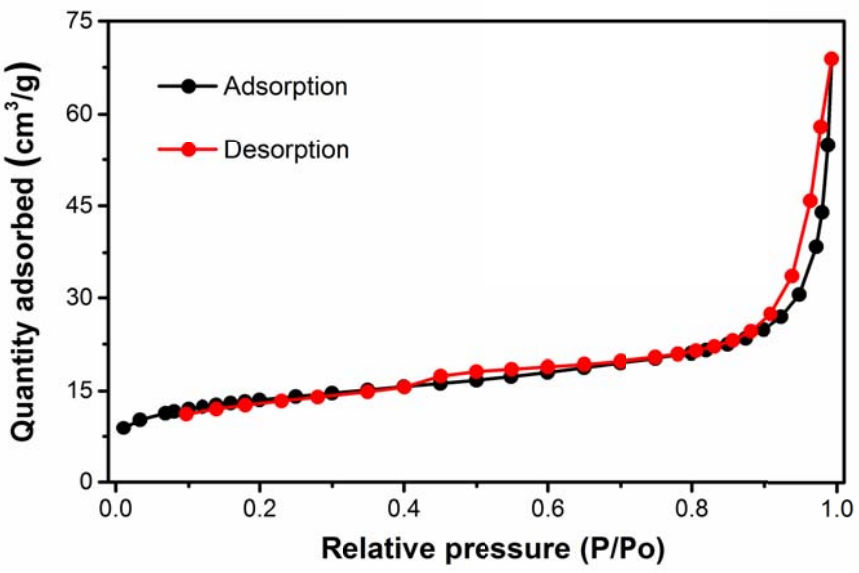

Fig. S1. Nitrogen adsorption-desorption isotherms of *h*-CeO_2.

S11. TGA curves

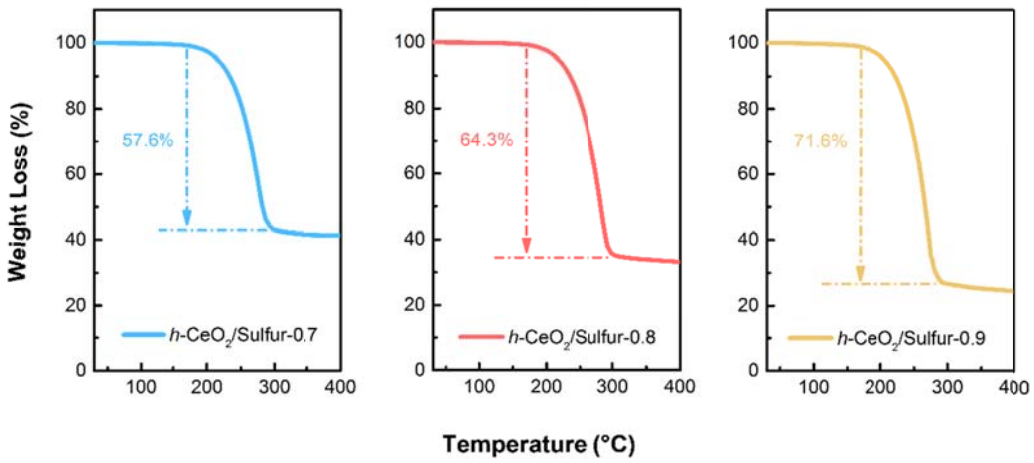

Fig. S2. TGA analysis of the *h*-CeO_2/Sulfur-x in air at a heating rate of 10 °C min^{-1}.

S12. Optimized geometries

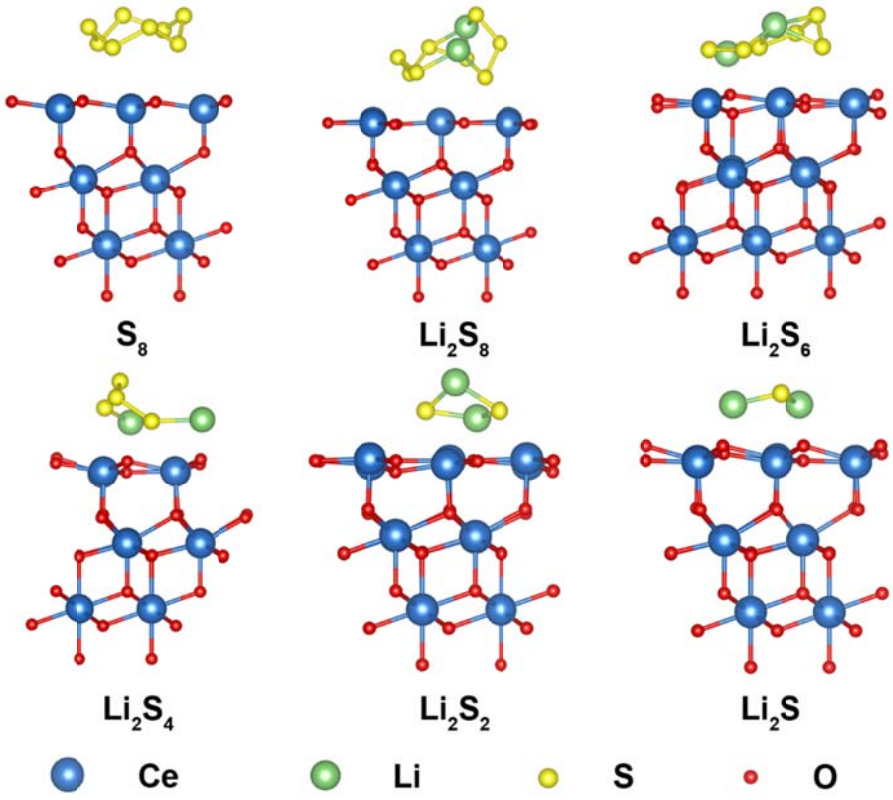

Fig. S3. Optimized geometries of S_8 and polysulfides on the ceria surface.

In our simulation, the CeO_2 (111) plane was selected and the adsorption energies were calculated between CeO_2 and lithium polysulfides.

S13. XPS spectra

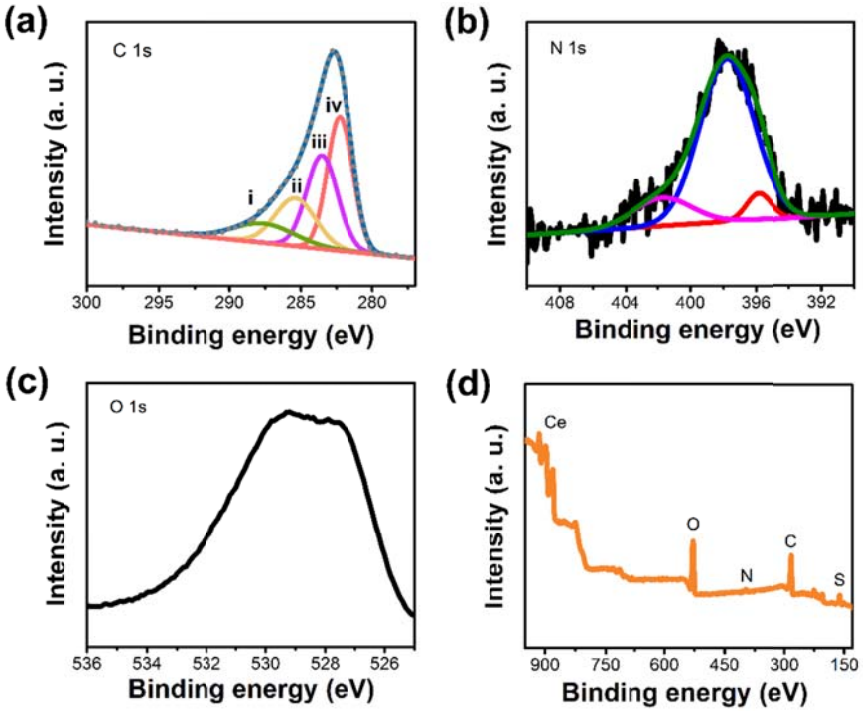

Fig. S4. XPS spectra of *h*-CeO_2/Sulfur-0.8: (a) C 1s, (b) N 1s, (c) O 1s and (d) survey spectrum.

The C 1s spectrum of *h*-CeO_2/Sulfur-0.8 sample was deconvoluted into four types of carbon species, labeled as i (287.7), ii (285.4), iii (283.5), iv (282.3 eV), respectively, indicating the existence of carbon atoms bonding with nitrogen, sulfur and oxygen heteroatoms. The peak at 285.4 eV was partially ascribed to C-S bonds. The N 1s spectrum was deconvoluted into three peaks at 395.8, 397.8, and 401.8 eV, respectively.

S14. Rate capabilities, charge/discharge and CV profiles

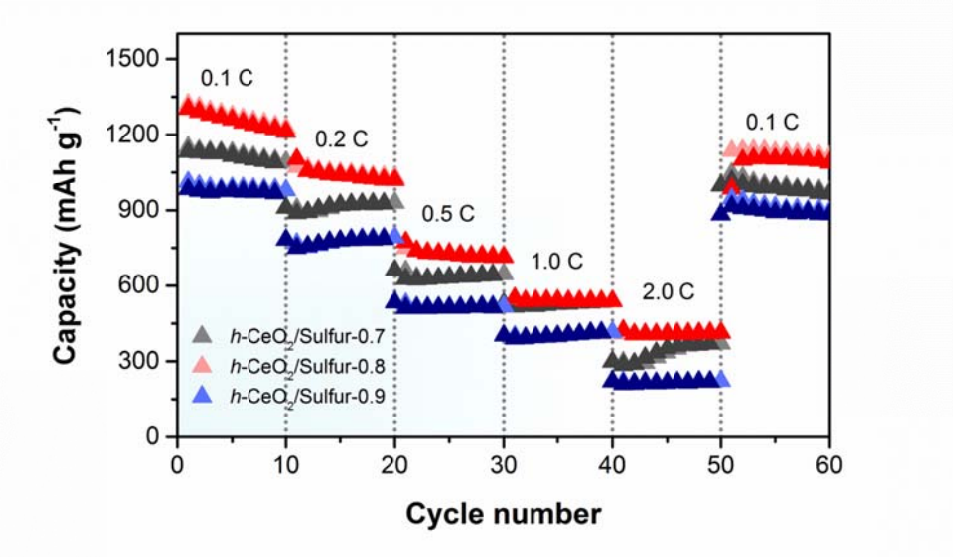

Fig. S5. Rate capabilities of *h*-CeO_2/Sulfur-0.7, *h*-CeO_2/Sulfur-0.8 and *h*-CeO_2/Sulfur-0.9.

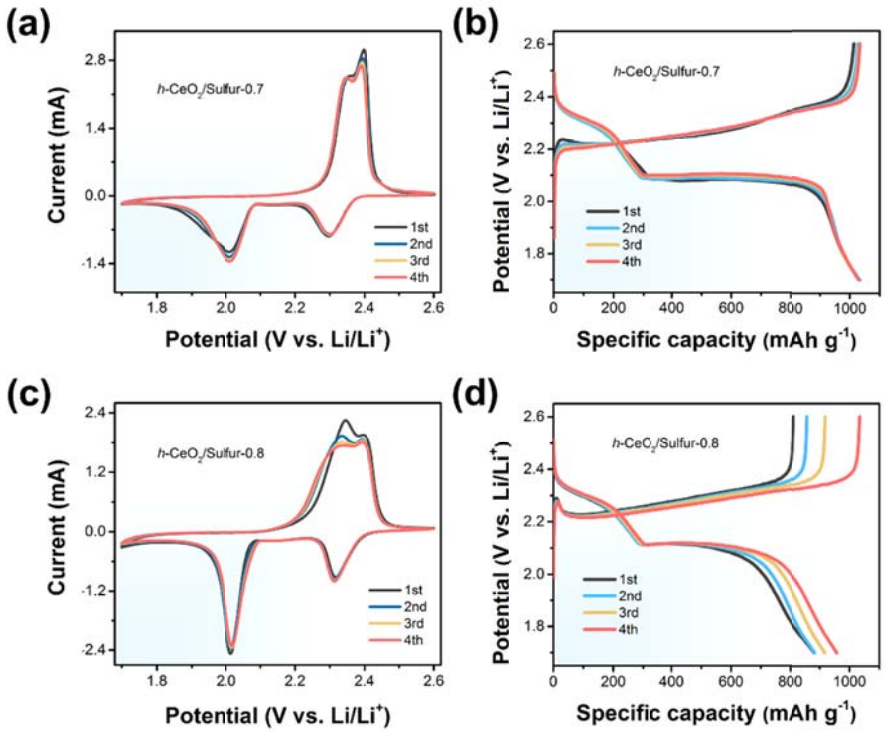

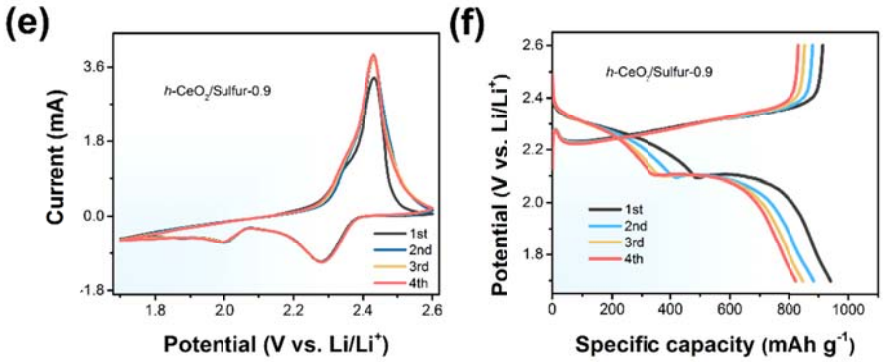

Fig. S6. The CV curves and charge/discharge profiles of *h*-CeO_2/Sulfur-x (x= 0.7, 0.8 and 0.9) cathode.

S15. Volumetric capacity and CV profiles

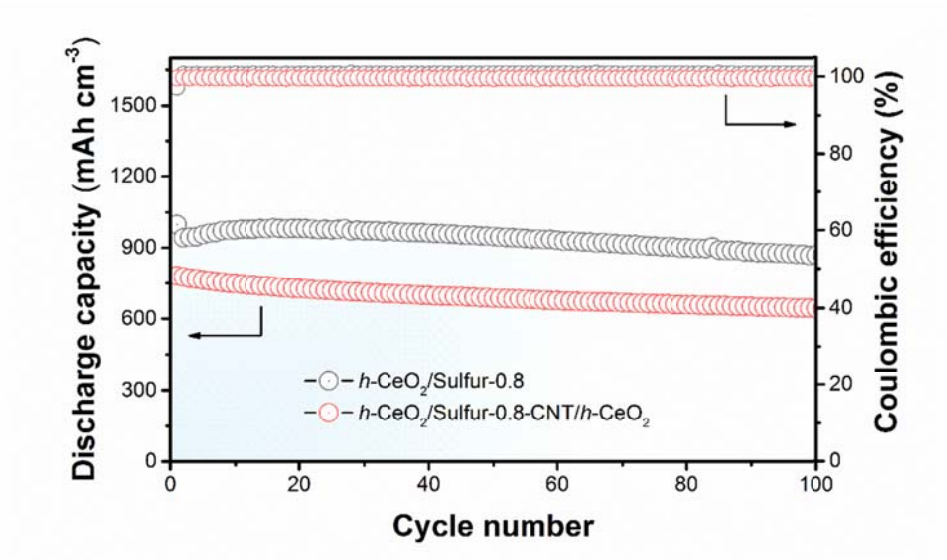

Fig. S7. Volumetric capacities of *h*-CeO_2/Sulfur-0.8 and *h*-CeO_2/Sulfur-0.8-CNT/h-CeO_2 interlayer at 0.5 C.

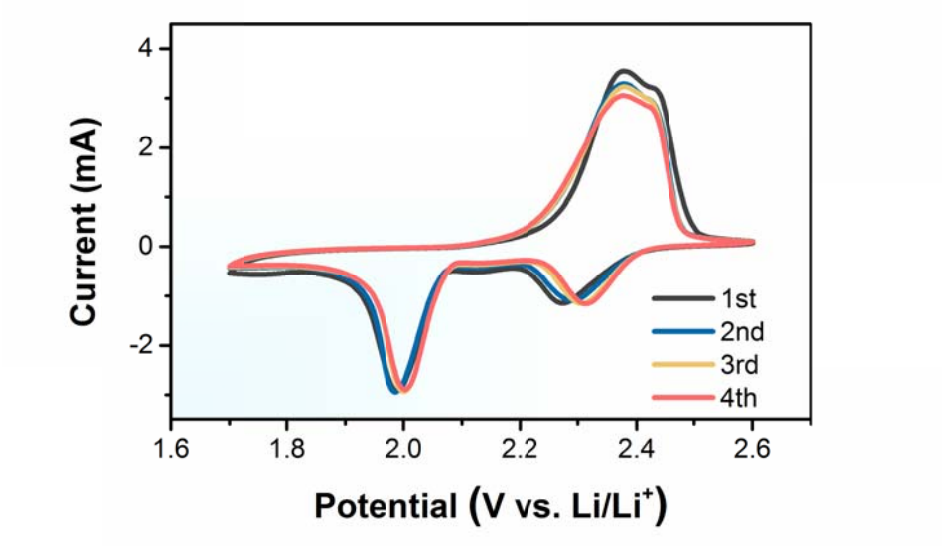

Fig. S8. CV profiles of *h*-CeO_2/Sulfur-0.8-CNT interlayer at a scan rate of 0.2 mV s^{-1}.

S16. Nyquist plots and equivalent circuit

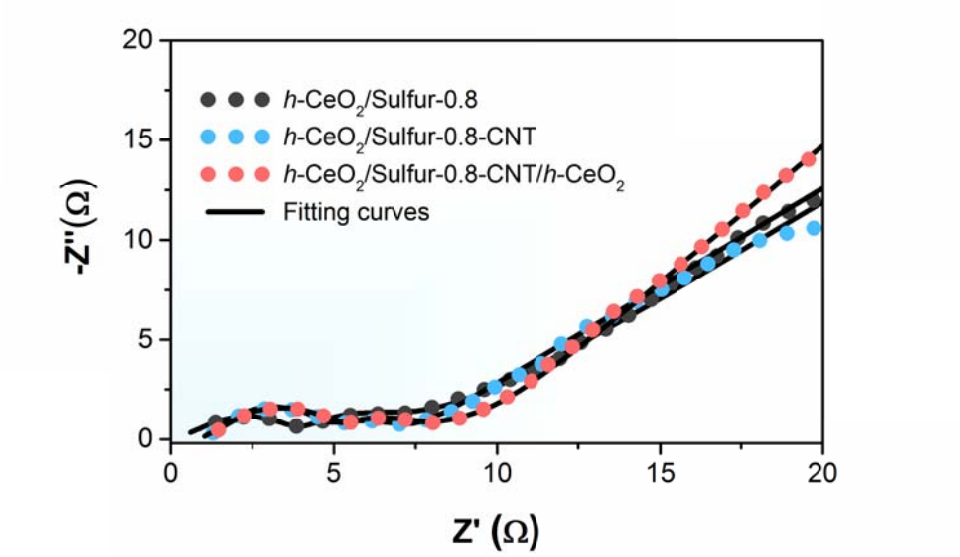

Fig. S9. Electrochemical impedance spectroscopy plots of three fresh cathodes for Li-S batteries.

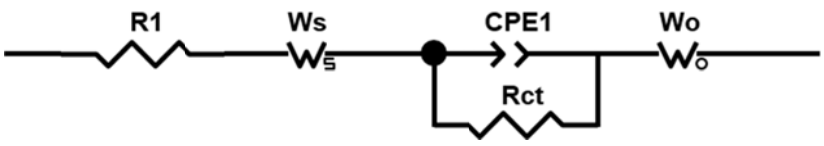

The above picture shows an equivalent circuit. R1: series resistance; Ws: adsorption impedance; Rct: charge-transfer resistance; Wo: the semi-infinite Warburg diffusion impedance.[5]

Table S1. EIS fitting results of the fresh cathodes

	***h*-CeO_2/Sulfur-0.8**	***h*-CeO_2/Sulfur-0.8-CNT**	***h*-CeO_2/Sulfur-0.8-CNT/*h*-CeO_2 interlayer**
R1	0.2825	0.8812	0.7396
Ws	3.135	3.460	3.961
Rct	3.237	2.838	2.093
Wo	10.43	0.0214	7.681

S17. The discharge/charge profiles of soft-packaged batteries

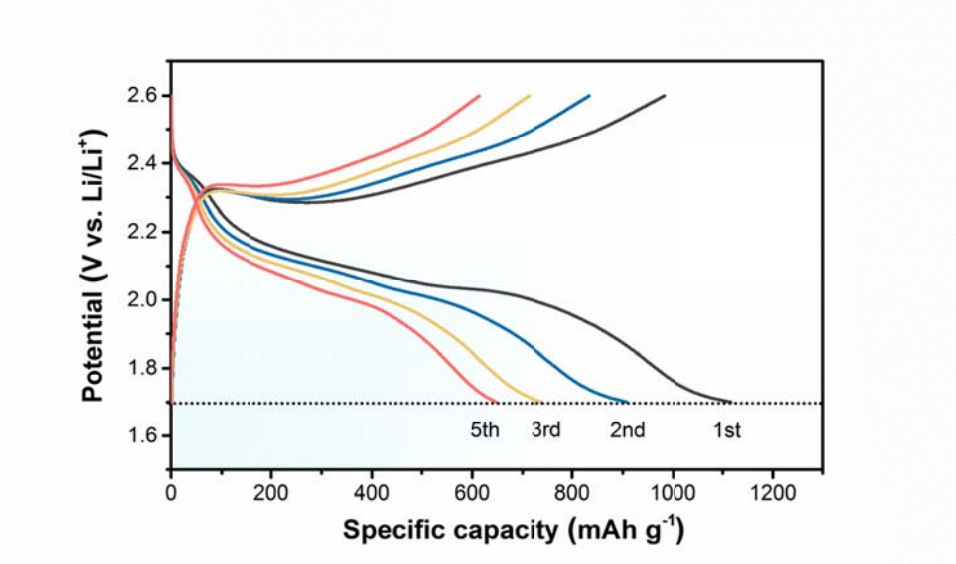

Fig. S10. Discharge/charge profiles of soft-packaged Li-S battery at various cycles (~20 cm^2 in area, sulfur loading is 0.84 mg cm^{-2}) with *h*-CeO_2/Sulfur-0.8-CNT/*h*-CeO_2 interlayer as the cathode at 0.1 C. The test was conducted with CHI600E.

S18. Schematic illustration of cathode configuration for Li–S batteries.

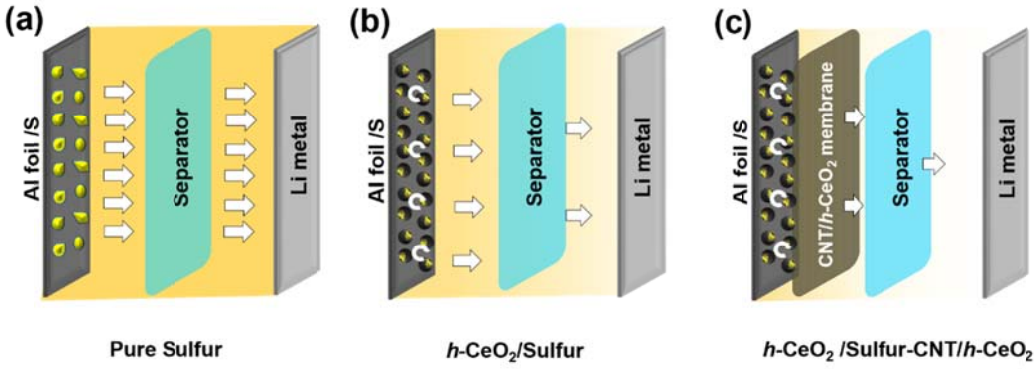

Fig. S11. Schematic illustration of Li–S batteries (1) with a pure sulfur electrode; (2) a *h*-CeO_2/Sulfur electrode; (3) a *h*-CeO_2/Sulfur cathode with CNT/*h*-CeO_2 interlayer cathode.

Conventional cathode in Li-S cells is often made of powder sulfur and nonpolar conductive additive, suffering from serious shuttle effect of polysulfides (Fig. S9a). The polysulfides generated during cycling process are highly polar and soluble. In this regard, it is necessary to introduce polar CeO_2 hollow spheres within the sulfur host. Nevertheless, the limited electrical conductivity of CeO_2 inevitably results in poor rate capability and fast capacity decay. In order to tackle this problem, a dopamine-derived carbon layer coated CeO_2 hollow sphere was prepared, which improves the electronic conductivity, ion permeability and charge transfer at the interface. Meanwhile, the hollow structure could tolerate the volume expansion. The diffusion and dissolution of polysulfides are remarkably suppressed, as shown in Fig. S9b. In addition, in order to further use the advantages of hollow CeO_2, a functional CNT/*h*-CeO_2 interlayer (Fig. S9c) was designed and inserted between the cathode and the separator via a simple layer-by-layer method.

S19. Comparison of electrochemical properties

Table S2. Comparison of electrochemical properties in previous reports about metal oxides

Polar host materials	Morphology	Voltage window (vs. Li^+)	Separator	Current density, Initial capacity, and Capacity retention	Sulfur infiltration method	Ref.
CeO_2	Hollow spheres	1.7-2.6 V	Celgard 2400	1 C, 876 mAh g^{-1}, 100 cycles, 85.7% 2 C, 761 mAh g^{-1}, 100 cycles, 87.8% 5 C, 644 mAh g^{-1}, 100 cycles, 92.4%	Melt-diffusion	**This work**
Al_2O_3	Ultrathin layer	1.5-2.8 V	Celgard 2400	0.5 C, 750 mAh g^{-1}, 100 cycles, 82%	Chemical co-precipitation	[6]
ZnO	laminates	1.0-2.8 V	Celgard 2325	0.2 C, 1414 mAh g^{-1}, 100 cycles, 47%	Melt-diffusion	[7]
MgO	Ultrathin layer	1.5-2.8 V	Celgard 2400	0.2 C, 923 mAh g^{-1}, 100 cycles, 83%	Chemical co-precipitation	[8]
V_2O_5	Hollow spheres	1.8-2.5 V	Not reported	0.2 C, 1000 mAh g^{-1}, 300 cycles, 82%	Melt-diffusion	[9]
VO_2	particles	1.8-3.0 V		0.2 C, ~1000 mAh g^{-1}, 150 cycles, 74%		
MoO_2	Mesoporous particles	1.7-2.8 V	Not reported	0.1 C, 1100 mAh g^{-1}, 100 cycles, 62%	Melt-diffusion	[10]
$Mg_{0.6}Ni_{0.4}O$	Nanoparticles	1.0-3.0 V	Celgard USA	0.1 C, 1545 mAh g^{-1}, 100 cycles, 79%	Melt-diffusion	[11]

Ti_4O_7	Particles	1.5-3.0 V	polypropylene membrane	0.5 C, 623 mAh g^{-1}, 250 cycles, 97%	Melt-diffusion	[12]
TiO_{2-x}	Inverse-opal 3D structure	1.8-2.6 V	Not reported	0.2 C, 1098 mAh g^{-1}, 200 cycles, 81%	Melt-diffusion	[13]
α-TiO_2	Particles	1.5-2.8 V	Not reported	0.5 C, 1201 mAh g^{-1}, 200 cycles, 73%	Melt-diffusion	[14]
β-TiO_2				0.5 C, 1135 mAh g^{-1}, 200 cycles, 62%		
γ-TiO_2				0.5 C, 1094 mAh g^{-1}, 200 cycles, 44%		
β-MnO_2	Mesoporous	1.0-3.0 V	Celgard 2400	0.05 mA cm^{-2}, ~2500 mAh g^{-1}, 100 cycles, ~60%	Melt-diffusion	[15]
La_2O_3	Nanoparticles	1.5-3.0 V	Celgard 2400	1 C, 1043 mAh g^{-1}, 100 cycles, 76%	Melt-diffusion	[16]
SnO_2	Hollow spheres	1.5-3.0 V	Celgard 2400	0.8 C, ~700 mAh g^{-1}, 100 cycles, ~71%	Melt-diffusion	[17]
WO_3	Nanoplates	1.7-2.6 V	Celgard 2400	0.5 C, 936.2 mAh g^{-1}, 300 cycles, 33.6%	Physical mixing and wet-impregnation	[18]
WO_{3-x}				0.5 C, 1028.5 mAh g^{-1}, 300 cycles, 59.5%		
ZrO_2	Nanoparticles	1.5-3.0 V	Celgard 2300	0.5 C, 829.4 mAh g^{-1}, 100 cycles, ~80%	Melt-diffusion	[19]
Fe_2O_3	Porous microcubes	1.0-3.0 V	Celgard 2400	0.5 C, ~920 mAh g^{-1}, 100 cycles, ~48%	Physical mixing	[20]

S20. References

1. G. Kresse, J. Furthmüller, *Phys. Rev*., 1996, **54**, 11169-11186.
2. J. P. Perdew, J. A. Chevary, S. H. Vosko, K. A. Jackson, M. R. Pederson, D. J. Singh, C. Fiolhais, *Phys. Rev. B*, 1992, **46**, 6671-6687.
3. J. Klimeš, D. R. Bowler, A. Michaelides, *J. Phys.: Cond. Matt*., 2010, **22**, 22201.
4. J. Klimeš, D. R. Bowler, A. Michaelides, *Phys. Rev. B*, 2011, 83.
5. Y. T. Liu, D. D. Han, L. Wang, G. R. Li, S. Liu, X. P. Gao, *Adv. Energy Mater*. 2019, 1803477.
6. M. Yu, W. Yuan, C. Li, J. D. Hong, G. Shi, *J. Mater. Chem. A*, 2014, **2**, 7360-7366.
7. X. Liang, Q. Song, Y. Liu, H. Liu, *Int. J. Electrochem. Sci.*, 2015, **10**, 9333-9341.
8. M. Yu, A. Wang, F. Tian, H. Song, Y. Wang, C. Li, J. D. Hong, G. Shi, *Nanoscale*, 2015, **7**, 5292-5298.
9. X. Liang, C. Y. Kwok, F. Lodi-Marzano, Q. Pang, M. Cuisinier, H. Huang, C. J. Hart, D. Houtarde, K. Kaup, H. Sommer, T. Brezesinski, J. Janek, L. F. Nazar, *Adv. Energy Mater*., 2015, **6**, 1501636.
10. Q. Qu, T. Gao, H. Zheng, Y. Wang, X. Li, X. Li, J. Chen, Y. Han, J. Shao, H. Zheng, *Adv. Mater. Interfaces*, 2015, **2**, 1500048.
11. Y. Zhang, Y. Zhao, A. Yermukhambetova, Z. Bakenov, P. Chen, *J. Mater. Chem. A*, 2013, **1**, 295-301.
12. X. Tao, J. Wang, Z. Ying, Q. Cai, G. Zheng, Y. Gan, H. Huang, Y. Xia, C. Liang, W. Zhang, Y. Cui, *Nano Lett*., 2014, **14**, 5288-5294.
13. Z. Liang, G. Zheng, W. Li, Z. W. Seh, H. Yao, K. Yan, D. Kong, Y. Cui, *ACS Nano*, 2014, **8**, 5249-5256.
14. S. Evers, T. Yim, L. F. Nazar, *J. Phys. Chem. C*, 2012, **116**, 19653-19658.
15. S. Wang, Z. Yang, H. Zhang, H. Tan, J. Yu, J. Wu, *Electrochim. Acta*, 2013, **106**, 307-311.
16. F. Sun, J. Wang, D. Long, W. Qiao, L. Ling, C. Lv, R. Cai, *J. Mater. Chem. A*, 2013, **1**, 13283-13289.
17. L. P. Zhang, Y. F. Wang, S. Q. Gou, J. H. Zeng, *J. Phys. Chem. C*, 2015, **119**, 28721-28727.
18. H. Lin, S. Zhang, T. Zhang, H. Ye, Q. Yao, G. W. Zheng, J. Y. Lee, *Adv. Energy Mater*., 2018, 1801868.
19. C. Wan, W. Wu, C. Wu, J. Xu, L. Guan, *RSC Adv*., 2015, **5**, 5102-5106.
20. C. Zhao, C. Shen, F. Xin, Z. Sun, W. Han, *Mater. Lett*., 2014, **137**, 52-55.